Integrated microwave photonic splitter with reconfigurable amplitude, phase and delay offsets

LEIMENG ZHUANG,[1,*] MAURIZIO BURLA,[2] CATERINA TADDEI,[3] CHRIS G. H. ROELOFFZEN,[4] MARCEL HOEKMAN,[5] ARNE LEINSE,[5] KLAUS –J. BOLLER,[3] AND ARTHUR J. LOWERY[1,6]

[1]*Electro-Photonics Laboratory, Department of Electrical and Computer Systems Engineering, Monash University, Clayton, VIC3800, Australia*
[2]*Institut National de la Recherche Scientifique (INRS-EMT), Montréal, Canada*
[3]*Laser Physics and Nonlinear Optics Group, University of Twente, P.O. Box 217, Enschede, 7500AE, The Netherlands*
[4]*SATRAX B.V., PO Box 456, Enschede, 7500AL, The Netherlands*
[5]*LioniX B.V., PO Box 456, Enschede, 7500AL, The Netherlands*
[6]*Centre for Ultrahigh-bandwidth Devices for Optical Systems (CUDOS), Australia*

**Corresponding author: leimeng.zhuang@monash.edu*

Received XX Month XXXX; revised XX Month, XXXX; accepted XX Month XXXX; posted XX Month XXXX (Doc. ID XXXXX); published XX Month XXXX

This work presents an integrated microwave photonics splitter with reconfigurable amplitude, phase, and delay offsets. The core components for this function are a dual-parallel Mach-Zehnder modulator, a deinterleaver, and tunable delay lines, all implemented using photonic integrated circuits. Using a demonstrator with an optical free spectral range of 25 GHz, we show experimentally the RF splitting function over two continuous bands, i.e. 0.9—11.6 GHz and 13.4—20 GHz. This result promises a deployable solution for creating wideband, reconfigurable RF splitters in integrated forms.

OCIS codes: *(060.5625) Radio frequency photonics; (130.3120) Integrated optics devices; (130.4815) Optical switching devices;*

http://dx.doi.org/10.1364/OL.99.099999

Integrated microwave photonics (IMWP) is providing a new and promising path for RF engineering by utilizing a broad range of photonic functions in integrated forms [1, 2]. Besides the unprecedented features of large instantaneous bandwidth, easy implementation of tuning, and reduced electromagnetic interference, IMWP enables RF functions with small size, weight, as well as power consumption, and allows for software-defined signal processing functions in one integrated device [3] (analogues to programmable electrical signal processors). This shows strong potential of commercial adoption in future RF communication and sensor systems and networks [4, 5].

Here, we present a wideband 1 × 2 RF splitter with reconfigurable amplitude, phase, and delay offsets between its two outputs, based on photonic integrated circuits (PICs). While difficult to achieve using conventional electronic integrated circuit technologies due to limited tuning capabilities [6—9], reconfigurable RF splitters can be realized in compact forms, resorting to IMWP technologies. These are a useful function with great application potential. For instance, the splitter can be applied for simultaneous generation of "I" and "Q" signals with a wide frequency coverage for coherent RF communication and radar systems [10]. Another example is to use the splitter as a reconfigurable feeding network for dual-linear antennas, which provides each antenna component an independent complex coefficient (arbitrary phase and amplitude) to enable electrically-controlled polarization-switching function [11] (e.g. switching between linear and circular polarizations by controlling the inter-component phase difference).

A number of microwave photonic phase shifters and delay lines have been introduced using various devices, such as spatial light modulators [12], fiber and waveguide gratings [13—15], semiconductor optical amplifiers [16, 17], waveguide ring resonators [18, 19], polarization modulators [20, 21], and fibers with stimulated Brillouin scattering [22, 23]. However, when applied into a 1 × 2 arbitrary-offset RF splitter, these approaches will in general lead to doubled system complexity for using two times phase shifters and/or delay lines. Besides, most of them will require independent controls of RF amplitude, phase, and delay for each output, incurring additional engineering effort. Recently, some of us presented the concept of a reconfigurable microwave photonic splitter allowing for arbitrary amplitude and phase offsets [24]. It utilizes a simple tuning mechanism in a dual-parallel Mach-Zehnder modulator (DPMZM) [25], and allows for broadband operation. However, the first demonstration of that concept comprises a bulky and expensive arrangement of discrete photonic devices, such as a spatial light modulator-based optical signal processor and two lasers.

In contrast, the IMWP approach we present in this work reduces the bulky system into a PIC-based solution that requires only one laser and provides delay offset as an additional dimension of reconfigurability. It improves the optical processing resolution to the sub-GHz regime, and has clear potential for single-chip integration as well as for functional extendibility. This owes to the fact that all the constituent components are common photonic integrated circuit building blocks and can be designed with reconfigurability [1, 2].

Figure 1 depicts the system configuration of the RF splitter. A CW laser provides an optical carrier frequency, f_{opt}. It is modulated by an RF input such that the output spectrum comprises of two RF sidebands and an optical carrier that has an independently adjustable phase. The process for achieving such modulation spectrum is shown in the insets (i) to (ii) of Fig. 1. For simplicity, we restrict here to the case of small

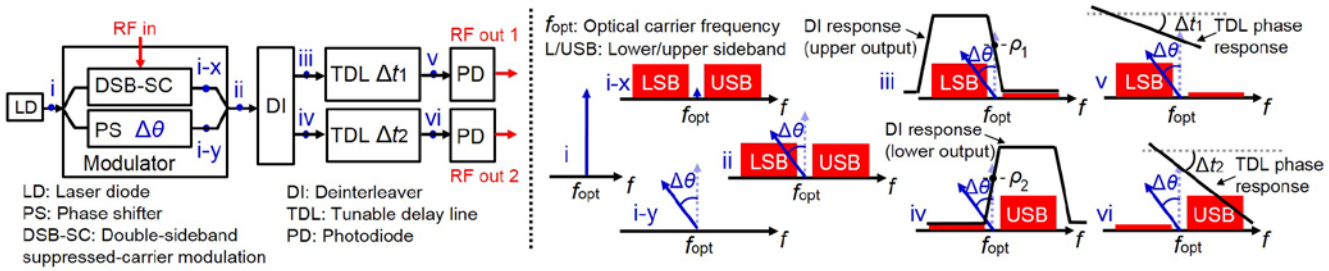

Fig. 1. System configuration and RF-to-RF signal flow of the RF splitter (left), with optical-spectrum illustrations (right).

signal modulation, so that only the first-order sidebands need to be taken into consideration [26]. Here, the optical carrier is first split into two separate paths. In one path, two RF sidebands are created by means of double-sideband suppressed-carrier (DSB-SC) modulation. In the other path, a phase control $\Delta\theta$ is applied to the optical carrier. Then, the recombination of the two paths results in the desired spectrum. Subsequently, the modulated optical signal is send to a dedicated deinterleaver, where the whole spectrum is cut into two parts and fed respectively to the two deinterleaver outputs. The filter response of the deinterleaver is designed such that each output let through one of the sidebands and a portion of the optical carrier as shown in the insets (iii) and (iv) of Fig. 1. In effect, each output contains a single-sideband-modulated optical carrier [18]. By means of direct detection, the beat product of the optical carrier and one sideband recovers the input RF signal, with an RF phase shift equal to the phase difference of the higher-frequency beat term relative to the lower-frequency beat term [26]. Then, the beat product of the optical carrier and lower sideband results in an RF phase shift, $\Delta\theta$, while the beat product of the upper sideband and optical carrier results in an opposite phase shift, $-\Delta\theta$, meaning an RF splitter phase offset of $2\Delta\theta$. When ρ_1 and $\rho_2 = 1-\rho_1$ are used to indicate the power splitting coefficients of the optical carrier, the ratio, $\beta = \rho_1/\rho_2$, governs the RF splitter amplitude offset. In addition, as shown in (v) and (vi) of Fig. 1, a pair of tunable delay lines providing two different delays, Δt_1 and Δt_2 (corresponding to two different phase slopes), are used to enable delay offset between the two outputs of the RF splitter.

Based on the small-signal assumption, the optical signals at the marked points of the system are given by

$$E_{\text{i-x}} = E_0 m(t)(\mathrm{e}^{-\mathrm{j}2\pi(f_{\text{opt}}-f_{\text{RF}})t} + \mathrm{e}^{-\mathrm{j}2\pi(f_{\text{opt}}+f_{\text{RF}})t}) \quad (1)$$

$$E_{\text{i-y}} = E_0(\mathrm{e}^{-\mathrm{j}(2\pi f_{\text{opt}}t+\Delta\theta)}) \quad (2)$$

$$E_{\text{ii}} = E_{\text{i-x}} + E_{\text{i-y}} = E_0(\mathrm{e}^{-\mathrm{j}(2\pi f_{\text{opt}}t+\Delta\theta)} + m(t)\mathrm{e}^{-\mathrm{j}2\pi(f_{\text{opt}}-f_{\text{RF}})t} + m(t)\mathrm{e}^{-\mathrm{j}2\pi(f_{\text{opt}}+f_{\text{RF}})t} \quad (3)$$

$$E_{\text{v}} = E_0(\sqrt{\rho_1}\,\mathrm{e}^{-\mathrm{j}(2\pi f_{\text{opt}}(t+\Delta t_1)+\Delta\theta)} + m(t)\mathrm{e}^{-\mathrm{j}2\pi(f_{\text{opt}}-f_{\text{RF}})(t+\Delta t_1)}) \quad (4)$$

$$E_{\text{vi}} = E_0(\sqrt{\rho_2}\,\mathrm{e}^{-\mathrm{j}(2\pi f_{\text{opt}}(t+\Delta t_2)+\Delta\theta)} + m(t)\mathrm{e}^{-\mathrm{j}2\pi(f_{\text{opt}}+f_{\text{RF}})(t+\Delta t_2)}) \quad (5)$$

where f_{opt} is the frequency of the optical carrier, $m(t)$ and f_{RF} are the complex amplitude and center frequency of the input RF signal, $s(t) = m(t)\cos(2\pi f_{\text{RF}}t)$, and E_0 represents the electric field amplitude of the optical input wave reduced by the losses in the signal paths. ρ_n (n = 1, 2) is the power splitting coefficient of the optical carrier for the two deinterleaver outputs, which is determined by where the optical carrier is positioned in the transition band of the deinterleaver, as shown in Fig. 1. Δt_n (n = 1, 2) is the time delay provided by the delay lines. For the sake of simplicity, without loss of generality, we ignore here the initial phases of the optical carrier and RF signals, and assume that the deinterleaver introduces no amplitude and phase distortions over the sidebands. Then the two photodetector outputs, I_{out1} and I_{out2}, can be derived from (4) and (5), respectively, as

$$I_{\text{out1}} = \sqrt{\rho_1}\eta m(t)\cos(2\pi f_{\text{RF}}(t+\Delta t_1)+\Delta\theta), \quad (6)$$

$$I_{\text{out2}} = \sqrt{\rho_2}\eta m(t)\cos(2\pi f_{\text{RF}}(t+\Delta t_2)-\Delta\theta), \quad (7)$$

where η represents a common RF amplitude factor determined by the input optical power and photodetector responsivity [26]. Evidently, such a system works as a 1 × 2 RF splitter with the amplitude, phase and delay offsets governed by the parameters, ρ_n, $\Delta\theta$, and Δt_n. Moreover, in the case that the deinterleaver provides periodic passbands along the frequency, the system explained above is able to operate at multiple RF bands within the bandwidths of the modulator and photodiode.

Figure 2 depicts our implementation of the modulator, deinterleaver and delay lines as photonic integrated circuits. For the DSB-SC modulator and carrier manipulation, we use a dual-parallel Mach-Zehnder modulator (DPMZM) comprising two Mach-Zehnder modulators (MZM1 and MZM2). As illustrated, in the upper arm, MZM1 is driven by the RF input signal and biased (via Bias 1) for DSB-SC modulation; in the lower arm, MZM2 and an independent optical phase shifter are biased (via Bias2 and Bias3, respectively) for controlling the amplitude and phase of the optical carrier.

The deinterleaver is realized via a Mach-Zehnder interferometer assisted with two ring resonators (2RAMZI), with their ring loops being twice as long as the differential arm length of the MZI [11]. The delay line uses a side-coupled integrated spaced sequence of resonators (SCISSOR) [27]. In terms of signal processing, these circuits can be modeled as digital filters [28], whose z-transform transfers are given by

$$\mathbf{H}_{\text{2RAMZI}} = \begin{bmatrix} H_{11}(z) & H_{12}(z) \\ H_{21}(z) & H_{22}(z) \end{bmatrix} = \delta \begin{bmatrix} \sqrt{1-\kappa_{\text{R}}} & -\mathrm{j}\sqrt{\kappa_{\text{R}}} \\ -\mathrm{j}\sqrt{\kappa_{\text{R}}} & \sqrt{1-\kappa_{\text{R}}} \end{bmatrix} \begin{bmatrix} A_{\text{U}}(z) & 0 \\ 0 & A_{\text{L}}(z) \end{bmatrix} \begin{bmatrix} \sqrt{1-\kappa_{\text{L}}} & -\mathrm{j}\sqrt{\kappa_{\text{L}}} \\ -\mathrm{j}\sqrt{\kappa_{\text{L}}} & \sqrt{1-\kappa_{\text{L}}} \end{bmatrix} \quad (8)$$

$$A_{\text{U}}(z) = \frac{\sqrt{1-\kappa_{\text{A}}} - \gamma^2 z^{-2} e^{-\mathrm{j}\phi_{\text{A}}}}{1-\sqrt{1-\kappa_{\text{A}}}\,\gamma^2 z^{-2} e^{-\mathrm{j}\phi_{\text{A}}}} \quad (9)$$

$$A_{\text{L}}(z) = \frac{\sqrt{1-\kappa_{\text{B}}} - \gamma^2 z^{-2} e^{-\mathrm{j}\phi_{\text{B}}}}{1-\sqrt{1-\kappa_{\text{B}}}\,\gamma^2 z^{-2} e^{-\mathrm{j}\phi_{\text{B}}}} \cdot \gamma z^{-1} e^{-\mathrm{j}\phi_{\text{C}}} \quad (10)$$

$$H_{\text{SCISSOR}}(z) = \chi \sum_{n=1}^{N} \frac{\sqrt{1-\kappa_n} - \gamma z^{-2} e^{-\mathrm{j}\phi_n}}{1-\sqrt{1-\kappa_n}\,\gamma z^{-2} e^{-\mathrm{j}\phi_n}} \quad (11)$$

where $z = \exp(-\mathrm{j}2\pi f/\Delta f_{\text{FSR}})$ represents the angular frequency normalized to the free spectral range, Δf_{FSR}, (FSR) of the circuit [28]. In the expressions, γ is the amplitude transmission coefficient determined by the waveguide loss, δ and χ are complex coefficients which account for the general insertion loss and phase shift introduced by the circuits, parameters κ and ϕ express the power coupling coefficient and phase shift, respectively. For providing circuit reconfigurability [1], κ and ϕ are controlled using phase tuning elements as illustrated in Fig. 2.

To provide an experimental verification, we realized a laboratory demonstrator of the proposed splitter. The setup uses a narrow bandwidth CW laser at 1.5 μm wavelength (AlnairLabs TLG-300M), a

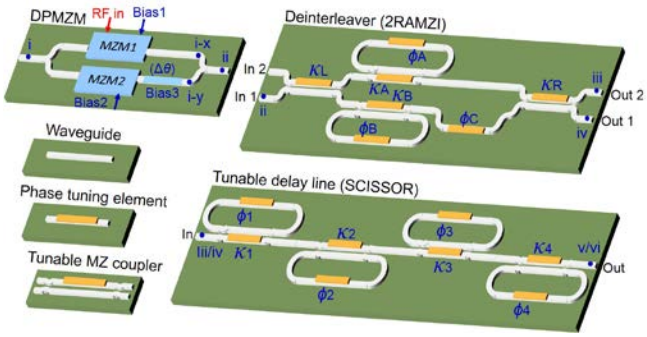

Fig. 2. Schematics of PIC implementations of the modulator, deinterleaver and delay line in the system shown in Fig. 1.

DPMZM (Sumitomo 40G DQPSK), and photodiodes (u²t XPRV2021A). The deinterleaver and delay lines comprising four cascaded ring resonators are fabricated on a single chip, in a commercial Si_3N_4 waveguide platform (TriPleX) [29, 30], with a common FSR design of 25 GHz. Chromium heaters on top of the waveguide enable thermal-optical phase tuning [1]. The chip coupling is optimized for TE polarization. The total fiber-to-fiber insertion loss amounts to 9 dB, dominated by two times fiber-chip coupling losses of about 4 dB/facet. However, this value is expected to decrease significantly, to about 1dB/facet [31] when a particular design of waveguide facet or interposer is used to optimize the coupling efficiency. Figure 3 depicts the waveguide mask layouts and measured frequency responses of the deinterleaver and delay line. The corresponding circuit parameters are listed in Table 1.

Table 1. Circuit parameters for the frequency responses in Fig. 3.

2RAMZI		SCISSOR		
	Value		Value (Delay 0 ns)	Value (Delay 0.2 ns)
κ_L	0.5	κ_1	0	0.70
κ_R	0.5	ϕ_1	Arbitrary	β-0.48π
κ_A	0.87	κ_2	0	0.76
ϕ_A	α	ϕ_2	Arbitrary	β-0.16π
κ_B	0.32	κ_3	0	0.76
ϕ_B	α	ϕ_3	Arbitrary	β+0.16π
ϕ_C	α+π/2	κ_4	0	0.70
		ϕ_4	Arbitrary	β+0.48π
α: phase for aligning the deinterleaver to optical carrier β: phase for aligning the delay band to the target RF sideband				

As shown in Fig. 3(c), the deinterleaver (2RAMZI) provides periodic passbands, allowing the system to operate at multiple RF bands. However, due to the bandwidth limitation of the modulator and photodiodes in our system, only two of these RF bands are selected in this work. This selection is motivated as follows. As explained in [11], the parameter setting in Table 1 configures the 2RAMZI into a 5th-order Chebyshev-Type-II filter. Such a filter is characterized by a flat passband with a -0.5 dB-bandwidth equal to 47% of the FSR, an equal-ripple stopband with suppression of 25 dB, and a sharp transition bandwidth (from -0.5 dB to -25 dB) equal to 7% of the filter -3dB bandwidth that accounts for half of the FSR. Based on our circuit FSR of 25 GHz, these features translate to a transition bandwidth of 0.9 GHz and an effective RF bandwidth of 10.7 GHz for each deinterleaver passband, considering the optical carrier is positioned within a transition band and both RF sidebands are covered in the -0.5 dB-passbands. Fig. 3(d) depicts the measured two group delay responses of the SCISSOR with delay values of 0 ns and 0.2 ns for a bandwidth of 13 GHz. These are configured to be wider than the deinterleaver passband and therefore guarantee that the entire RF sideband is covered in the delay band. When required, a larger delay tuning range can be provided by increasing the number of ring resonators [1, 27, 28]. Due to the loss in the waveguide, the total loss of the delay line increases in a near-linear manner with the delay value [30]. In our experiment, a delay of 0.2 ns induces a loss about 0.5 dB.

With the DPMZM, deinterleaver, and delay lines properly configured, we performed a measurement of the RF transmission of the demonstrator system (scattering parameter S_{21}), using a vector network analyzer (Anritsu 37247D). As shown in Fig. 3c, the optical carrier was initially positioned in the middle between the transition bands of the two deinterleaver outputs, i.e., at the -3-dB position with respect to both H_{11} and H_{21}, corresponding to equal optical carrier splitting coefficients, $\rho_1 = \rho_2$ (Fig. 1). Two RF sweeping bands were used, i.e. 0.9 to 11.6 GHz and 13.4 to 20 GHz (limited by the maximum frequency of the measurement equipment). The measurement system was calibrated to remove the effect of the RF cables. Figure 4(a) depicts the RF phase responses of the system, where the initial phase offset between the two outputs is removed for clarity. For this measurement, the delay lines were bypassed by using the 0-ns setting, and RF phase offset with a continuous and full tuning range of 2π was demonstrated by continuously changing the optical carrier phase via Bias3 of the modulator. Figure 4(b) depicts the RF power responses of the system. Here, we demonstrate the function of a tunable amplitude offset, which was performed by varying ρ_1 and ρ_2 through frequency-shifting the deinterleaver response (equivalent to changing the position of the optical carrier in the transition band of the deinterleaver). When the deinterleaver response (Fig. 3c) shifts to a lower frequency, ρ_1 for Out 1 decreases as the optical carrier becomes closer to the stopband of H_{21}, whereas ρ_2 for Out 2 increases as the optical carrier becomes closer to the passband of H_{11}. This will be vice versa when the deinterleaver response shifts to a higher frequency. The frequency shift was implemented using the heaters that control $\phi_{A\text{-}C}$. Figure 4(c) depicts the effect of the delay line. As an example, an output was provided with an additional delay of 0.2 ns as shown in Fig. 3d. Then, an RF phase slope difference is obtained as expected between the two outputs. The delay change was performed using the heaters for $\kappa_{1\text{-}4}$ and $\phi_{1\text{-}4}$.

The results in Fig. 4 clearly prove the continuous reconfigurability of the amplitude, phase, and delay offsets of the RF splitter function. As all the tuning elements in the system (modulator biases and circuit heaters) are driven by DC voltages, a simple multi-channel DC supply can be used for system configuration. For the voltage control, a micro-controller and a look-up table can be employed as a possible approach

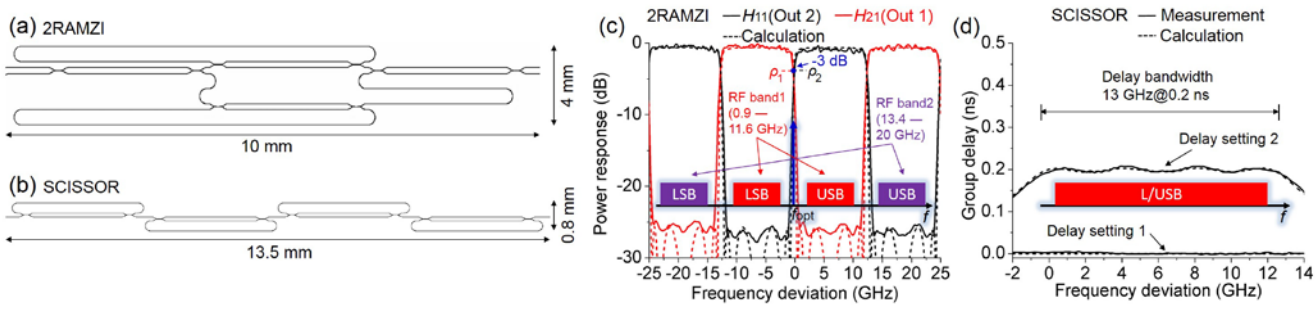

Fig. 3. (a, b) waveguide mask layouts of the 2RAMZI and 4-ring SCISSOR; (c) measured power response of the 2RAMZI, with illustration of the frequency alignment with respect to the optical signal spectrum; (d) two measured group delay responses of the SCISSOR.

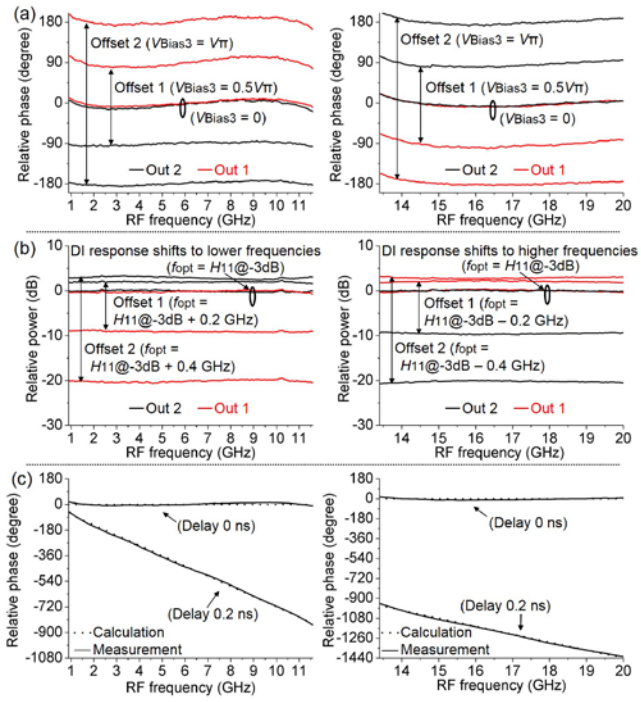

Fig. 4. RF transmission measurements (scattering parameter S_{21}) of the system for RF bands 0.9 to 11.6 GHz and 13.4 to 20 GHz: (a) continuous tuning of phase responses ($V\pi$: modulator DC halfwave voltage), (b) continuous tuning of power responses, and (c) continuous tuning of phase responses showing the delay effect.

for the parameter tuning process. Our demonstrator chip has a power dissipation about 150 mW/heater (using the heater design as in [1, 18, 19, 30]). However, for such passive-function PICs, alternative implementations of phase tuning have been demonstrated recently with multiple-orders-of-magnitude reductions of power dissipation [32, 33], which are highly promising for practical applications.

The proposed system is in nature a microwave photonic link, therefore achieving a system gain and dynamic range that outperform the current all-electronics RF processing systems remains a challenge [34]. These issues require further improvement of the optoelectronic components [26]. In terms of device realization, the proposed system has the potential to be fully integrated on the chip level. This can be seen from a number of previous works showing the integration of similar PIC building blocks by means of micro-assembly of chips of different technologies [31, 35, 36] or monolithic integration on one waveguide platform such as InP [37].

In conclusion, we have demonstrated a wideband 1 × 2 RF splitter with reconfigurable amplitude, phase and delay offsets. The system is expected to be realized as a stand-alone device and have great application potential in the wideband RF communication systems.

Funding. This work is funded by Australian Research Council Laureate fellowship (FL13010041) and Dutch Agentschap NL IOP project PROMIS2DAY (IPD12009).

References

1. C. G. H. Roeloffzen, L. Zhuang, C. Taddei, A. Leinse, R. G. Heideman, P. W. L. van Dijk, R. M. Oldenbeuving, D. A. I. Marpaung, M. Burla, and K. –J. Boller, Opt. Express **21**(19), 22937 (2013).
2. D. A. I. Marpaung, C. G. H. Roeloffzen, R. G. Heideman, A. Leinse, S. Sales, and J. Capmany, Laser Photonic Rev. **7**, 506 (2013).
3. L. Zhuang, C. G. H. Roloffzen, M. Hoekman, K.-J. Boller and A. J. Lowery, Optica **2**(10), 854 (2015).
4. J. Capmay and D. Novak, Nat. Photonics **1**(6), 319 (2007).
5. J. P. Yao, J. Lightwave Technol. **27**(3), 314 (2009).
6. J. Long, C. Li, W. Cui, J. Huangfu, and L. Ran, IEEE Microw. Wireless Compon. Lett. **21**, 74 (2011).
7. A. Velez, F. Aznar, M. Durán-Sindreu, J. Bonache, and F. Martin, IEEE Microw. Antennas Propag. **5**, 277 (2011).
8. V. Sekar, M. Armendariz, K. A. Entesari, IEEE Trans. Microwave Theory Tech. **59**, 866 (2011).
9. M. R. Rafique, T. Ohki, B. Banik, H. Engseth, P. Linner, and A. Herr, Supercond. Sci. Technol. **21**, 075004 (2008).
10. P. Ghelfi, F. Laghezza, F. Scotti, G. Serafino, A. Capria, S. Pinna, D. onori, C. Porzi, M. Scaffardi, A. Malacarne, V. Vercesi, E. Lazzeri, F. Berizzi, and A. Bogoni, Nature **501**(4792), 341 (2014).
11. L. Zhuang, W. P. Beeker, A. Leinse, R. G. Heideman, P. W. L. van Dijk, and C. G. H. Roeloffzen, Opt. Express **21**(3), 3114 (2013).
12. T. X. H. Huang, X. Yi, and R. A. Minasian, Opt. Lett. **36**(22), 4440 (2011).
13. W. Liu and J. Yao, Opt. Lett. **39**(4), 922 (2014).
14. H. Shahoei and J. Yao, Opt. Express **30**(13), 14009 (2012).
15. M. Burla, L. Romero Cortés, M. Li, X. Wang, L. Chrostowski, and J. Azaña, Opt. Lett. **39**(21), 6181 (2014).
16. H. Chen, M. Sun, Y, Ding, and X. Sun, Opt. Lett. **38**(17), 3272 (2013).
17. J. Sancho, J. Lloret, I. Gasulla, S. Sales, and J. Capmany, Opt. Express **19**(18), 17421 (2011).
18. M. Burla, D. A. I. Marpaung, L. Zhuang, C. G. H. Roeloffzen, M. R. Khan, A. Leinse, M. Hoekman, and R. G. Heideman, Opt. Express **19**, 21475 (2011).
19. L. Zhuang, M. R. Khan, W. P. Beeker, A. Leinse, R. G. Heideman, and C. G. H. Roeloffzen, Opt. Express **20**(24), 26499 (2012).
20. S. Pan, Y. Zhang, Opt. Lett. **37**(21), 4483 (2012).
21. W. Li, W. Zhang, and J. Yao, Opt. Express **20**(28), 29838 (2012).
22. X. Sun, S. Fu, K. Xu, J. Zhou, P. Shum, J. Yin, X. Hong, J. Wu, and J. Lin, IEEE Trans. MTT **58**(11), 3206 (2010).
23. A. Loayssa and F. J. Lahoz, IEEE Photon. Techno. Lett. **18**(1), 208 (2006).
24. L. Zhuang, B. Corcoran, C. Zhu, and A. J. Lowery, IEEE Photon. Technol. Lett. **21**(26), 2122 (2014).
25. W. Li, N. H. Zhu and L. X. Wang, IEEE Photon. J. **3**(3), 462 (2011).
26. C. H. Cox, Analog optical links: theory and practice, Cambridge (2004).
27. J. Cardenas, M. A. Foster, N. Sherwood-Droz, C. B. Poitras, H. L. R. Lira, B. Zhang, A. L. Gaeta, J. B. Khurgin, P. Morton, and M. Lipson, Opt. Express **18**(25), 26525 (2010).
28. C. K. Madsen and J. H. Zhao, Optical filter design and analysis: a signal processing approach, Wiley (1999).
29. K. Wörhoff, R. G. Heideman, A. Leinse and M. Hoekman, Adv. Opt. Techn. **4**(2), 189 (2015).
30. L. Zhuang, D. A. I. Marpaung, M. Burla, W. P. Beeker, A. Leinse, R. G. Heideman and C. G. H. Roeloffzen , Opt. Express **19**(23), 23162 (2010).
31. Y. Fan, R. M. Oldenbeuving, E. J. Klein, C. J. Lee, H. Song, M. R. H. Khan, H. L. Offerhaus, P. J. M. van der Slot and K.-J. Boller, Proc. SPIE91351B (2014).
32. J. Capmany, D. Domenech and P. Muñoz, IEEE Photon. J. **7**(2), 2700609 (2015).
33. N. Hosseini, R. Dekker, M. Hoekman, M. Dekkers, J. Bos, A. Leinse and R. G. Heideman, Opt. Express **23**(11), 14018 (2015).
34. E. I. Ackerman, G. Betts, W. K. Burns, J. C. Campbell, C. H. III Cox, N. Duan, J. L. Prince, M. D. Regan and H. V. Roussell, Proc. of the International Microwave Symposium, 51 (2007).
35. R. M. Oldenbeuving, E. J. Klein, H. L. Offerhaus, C. J. Lee, H. Song and K. –J. Boller, Laser Phys. Lett. **10,** 015804 (2013).
36. L. Zhuang, C. Taddei, M. Hoekman, D. Ronald, C. G. H. Roeloffzen, K. –J. Boller and A. J. Lowery, Proc. of the Asia Communications and photonics Conference, ATh1F.3 (2014).
37. M. Smit, J. van der Tol, and M. Hill, Laser & Photon. Rev. **6**(1), 1 (2011).

References

1. C. G. H. Roeloffzen, L. Zhuang, C. Taddei, A. Leinse, R. G. Heideman, P. W. L. van Dijk, R. M. Oldenbeuving, D. A. I. Marpaung, M. Burla, and K. –J. Boller, "Silicon nitride microwave photonic circuits," Opt. Express, vol. 21, no. 19, pp. 22937-22961, 2013
2. D. A. I. Marpaung, C. G. H. Roeloffzen, R. G. Heideman, A. Leinse, S. Sales, and J. Capmany, "Integrated microwave photonics," Laser Photonic Rev., vol. 7, pp. 506-538, 2013.
3. L. Zhuang, C. G. H. Roeloffzen, M. Hoekman, K.-J. Boller and A. J. Lowery, "Programmable photonic signal processor chip for RF applications", vol. 2, no. 10, pp. 854-859, 2015.
4. J. Capmay and D. Novak, "Microwave photonics combines two worlds," Nat. Photonics, vol. 1, no. 6, pp. 319-330, 2007.
5. J. P. Yao, "Microwave photonics," J. Lightwave Technol., vol. 27, no. 3, pp. 314-335, 2009.
6. J. Long, C. Li, W. Cui, J. Huangfu, and L. Ran, "A tunable microstrip bandpass filter with two independently adjustable transmission zeros," IEEE Microw. Wireless Compon. Lett., vol. 21, pp. 74-76, 2011.
7. A. Velez, F. Aznar, M. Durán-Sindreu, J. Bonache, and F. Martin, "Tunable coplanar waveguide band-stop and band-pass filters based on open split ring resonators and open complementary split ring resonators," IEEE Microw. Antennas Propag., vol. 5, pp. 277-281, 2011.
8. V. Sekar, M. Armendariz, K. A. Entesari, "A 1.2-1.6-GHz substrate-integrated-waveguide RF MEMS tunable filter," IEEE Trans. Microwave Theory Tech., vol. 59, pp. 866-876, 2011.
9. M. R. Rafique, T. Ohki, B. Banik, H. Engseth, P. Linner, and A. Herr, "Miniaturized superconducting microwave filters," Supercond. Sci. Technol., vol. 21, 075004, 2008.
10. P. Ghelfi, F. Laghezza, F. Scotti, G. Serafino, A. Capria, S. Pinna, D. onori, C. Porzi, M. Scaffardi, A. Malacarne, V. Vercesi, E. Lazzeri, F. Berizzi, and A. Bogoni, "A fully photonic-based coherent radar system," Nature, vol. 501, no. 4792, pp. 341-345, 2014.
11. L. Zhuang, W. P. Beeker, A. Leinse, R. G. Heideman, P. W. L. van Dijk, and C. G. H. Roeloffzen, "Novel wideband microwave photonic polarization network using a fully-reconfigurable photonic waveguide interleaver with a two-ring resonator-assisted asymmetric Mach-Zehnder structure," Opt. Express, vol. 21, no. 3, pp. 3114-3124, 2013.
12. T. X. H. Huang, X. Yi, and R. A. Minasian, "Microwave Photonic quadrature filter based on an all-optical programmable Hilbert transformer," Opt. Lett., vol. 36, no. 22, pp. 4440-4442, 2011.
13. W. Liu and J. Yao, "Ultra-wideband microwave photonic phase shifter with a 360° tunable phase shift based on an erbium-ytterbium co-doped linearly chirped FBG," Opt. Lett., vol. 39, no. 4, pp. 922-924, 2014.
14. H. Shahoei and J. Yao, "Tunable microwave photonic phase shifter based on slow and fast light effects in a tilted fiber bragg grating," Opt. Express, vol. 30, no. 13, pp. 14009-14014, 2012.
15. M. Burla, L. Romero Cortés, M. Li, X. Wang, L. Chrostowski, and J. Azaña, "On-chip programmable ultra-wideband microwave photonic phase shifter and true time delay unit," Opt. Lett., vol. 39, no. 21, pp. 6181-6184, 2014.
16. H. Chen, M. Sun, Y, Ding, and X. Sun, "Microwave photonic phase shifter based on birefringence effects in a semiconductor optical amplifier," Opt. Lett., vol. 38, no. 17, pp. 3272-3274, 2013.
17. J. Sancho, J. Lloret, I. Gasulla, S. Sales, and J. Capmany, "Fully tunable 360° microwave photonic phase shifter based on a single semiconductor optical amplifier," Opt. Express, vol. 19, no. 18, pp. 17421-17426, 2011.
18. M. Burla, D. A. I. Marpaung, L. Zhuang, C. G. H. Roeloffzen, M. R. Khan, A. Leinse, M. Hoekman, and R. G. Heideman, "On-chip CMOS compatible reconfigurable optical delay line with separate carrier tuning for microwave photonic signal processing," Opt. Express, vol. 19, no. 22, pp. 21475-21484, 2011.
19. L. Zhuang, M. R. Khan, W. P. Beeker, A. Leinse, R. G. Heideman, and C. G. H. Roeloffzen, "Novel microwave photonic fractional Hilbert transformer using on a ring resonator-based optical all-pass filter," Opt. Express, vol. 20, no. 24, pp. 26499-26510, 2012.
20. S. Pan, Y. Zhang, "Tunable and wideband microwave photonic phase shifter based on a single-sideband polarization modulator and polarizer," Opt. Lett., vol. 37, no. 21, pp. 4483-4485, 2012.
21. W. Li, W. Zhang, and J. Yao, "A wideband 360° photonic-assisted microwave phase shifter using a polarization modulator and a polarization-maintaining fiber Bragg grating," Opt. Express, vol. 20, no. 28, pp. 29838-29843, 2012.
22. X. Sun, S. Fu, K. Xu, J. Zhou, P. Shum, J. Yin, X. Hong, J. Wu, and J. Lin, "Photonic RF phase shifter based on a vector-sum technique using stimulated Brillouin scattering in dispersion shifted fiber," IEEE Trans. MTT, vol. 58, no. 11, pp. 3206-3212, 2010.
23. A. Loayssa and F. J. Lahoz, "Broad-band RF photonic phase shifter based on stimulated Brillouin scattering and single-sideband modulation," IEEE Photon. Techno. Lett., vol. 18, no. 1, pp. 208-210, 2006.
24. L. Zhuang, B. Corcoran, C. Zhu, and A. J. Lowery, "Photonic high-bandwidth RF splitter with arbitrary amplitude and phase offset," IEEE Photon. Technol. Lett., vol. 21, no. 26, pp. 2122-2125, 2014.
25. W. Li, N. H. Zhu and L. X. Wang, "Continuously tunable microwave photonic notch filter with complex coefficient," IEEE Photon. J., vol. 3, no. 3, pp. 462-467, 2011.
26. C. H. Cox, Analog optical links: theory and practice, Cambridge, 2004.
27. J. Cardenas, M. A. Foster, N. Sherwood-Droz, C. B. Poitras, H. L. R. Lira, B. Zhang, A. L. Gaeta, J. B. Khurgin, P. Morton, and M. Lipson, "Wide-bandwidth continuously tunable optical delaly line suing silicon microring resonators," Opt. Express, vol. 18, no. 25, pp. 26525-26534, 2010.
28. C. K. Madsen and J. H. Zhao, Optical filter design and analysis: a signal processing approach, Wiley, 1999.
29. K. Wörhoff, R. G. Heideman, A. Leinse and M. Hoekman, "TriPleX: a versatile dielectric photonic platform," Adv. Opt. Techn., vol. 4, no. 2, pp. 189-207, 2015.
30. L. Zhuang, D. A. I. Marpaung, M. Burla, W. P. Beeker, A. Leinse, R. G. Heideman and C. G. H. Roeloffzen, "Low-loss, high-index-contrast Si_3N_4/SiO_2 optical waveguides for optical delay lines in microwave photonics signal processing," Opt. Express, vol. 19, no. 23, pp. 23162-23170, 2010.
31. Y. Fan, R. M. Oldenbeuving, E. J. Klein, C. J. Lee, H. Song, M. R. H. Khan, H. L. Offerhaus, P. J. M. van der Slot and K.-J. Boller, "A hybrid semiconductor-glass waveguide laser," Proc. SPIE 9135, Laser Sources and Applications II, 91351B, Brussels, Belgium, May 2014.
32. J. Capmany, D. Domenech and P. Muñoz, "Silicon graphene reconfigurable CROWS and SCISSORS," IEEE Photon. J., vol. 7, no. 2, 2700609, 2015.
33. N. Hosseini, R. Dekker, M. Hoekman, M. Dekkers, J. Bos, A. Leinse and R. G. Heideman, "Stress-optic modulator in TriPleX platform using a ezoelectric lead zirconate titanate (PZT) thin film," Opt. Express, vol. 23, no. 11, pp. 14018-14026, 2015.
34. E. I. Ackerman, G. Betts, W. K. Burns, J. C. Campbell, C. H. III Cox, N. Duan, J. L. Prince, M. D. Regan and H. V. Roussell, "Signal-to-noise performance of two analog photonic links using different noise reduction techniques," Proc. of the International Microwave Symposium, pp. 51–54, 2007.
35. R. M. Oldenbeuving, E. J. Klein, H. L. Offerhaus, C. J. Lee, H. Song and K. –J. Boller, "25 kHz narrow spectral bandwidth of a wavelength tunable diode laser with a short waveguide-based external cavity," Laser Phys. Lett., vol. 10, 015804, 2013.
36. L. Zhuang, C. Taddei, M. Hoekman, D. Ronald, C. G. H. Roeloffzen, K. –J. Boller and A. J. Lowery, "Integrated photonic signal processor for microwave photonics and optical communications: a progress review in TriPleX™ Si_3N_4 waveguide technology," Prof. of the Asia Communications and Photonics conference, ATh1F.3, 2014.
37. M. Smit, J. van der Tol, and M. Hill, "Moore's law in photonics," Laser & Photon. Rev., vol. 6, no. 1, pp.1-13, 2011.